Waste Biomass Valor (2016) 7:551–557
DOI 10.1007/s12649-015-9458-0

REVIEW

Three-Dimensional Activated Carbon Recycled from Rotten Potatoes for High-performance Supercapacitors

Xueyang Chen[1] · Kai Wu[1] · Biao Gao[1] · Qiaoyu Xiao[1] · Jinhan Kong[1] · Qi Xiong[1] · Xiang Peng[1] · Xuming Zhang[1] · Jijiang Fu[1]

Received: 16 July 2015 / Accepted: 26 November 2015 / Published online: 15 December 2015

Abstract Carbon material derived from waste biomass for supercapacitor applications has been widely investigated because of its low cost and environmental friendly. In this paper, rotten potato was selected as the precursor to prepare three-dimensional (3D) activated carbon (AC) after hydrothermal treatment, carbonization and activation of KOH. Benefiting from large specific surface area, 3D interconnected macropore framework incorporating with meso-/micropore and the intrinsic good conductivity, the rotten potato-derived AC achieves a relatively high capacitance of 269 F g^{-1} (1 A g^{-1}), desirable rate performance and superior cycling stability. More importantly, the assembled symmetric device delivers a high specific capacitance (48 F g^{-1}) and a high energy density (4.27 Wh kg^{-1}) at a current density of 1 A g^{-1}. The result indicates a low-cost and facile approach for high-performance AC based on waste biomass source implying commercial potential in supercapacitor applications.

Keywords Waste biomass · Rotten potato · Activated carbon · Porous · Supercapacitors

✉ Biao Gao
gaobiao@wust.edu.cn

✉ Xuming Zhang
xumzhang@wust.edu.cn

[1] The State Key Laboratory of Refractories and Metallurgy, Wuhan University of Science and Technology, Wuhan 430081, People's Republic of China

Introduction

High-performance supercapacitors have been paid much attention in recent years owing to its high power density, high charge and discharge rate, excellent low temperature operation performance as well as long cycle life, and been widely applied to portable electronics, medical and military devices, and hybrid electric vehicles [1–5]. Generally, supercapacitors are classified into two typical forms according to the charge storage mechanism: one is electric double-layer capacitors (EDLCs), and the other is pseudocapacitors. In comparison with pseudocapacitors, EDLCs mainly based on carbon materials with large specific surface, such as activated carbon (AC), carbon nanotubes and graphene, which store charge or ions in the double layer on the surface. EDLCs own high power density and high reversibility for extraordinary cycle stability. AC, a commercial product often produced by petrochemical industry, has been widely used as the electrode additive for supercapacitor application due to its high specific surface area and good electric conductivity [6–8]. However, with the depletion of the fossil source and corresponding increased environmental pollution, to find a replaced low-cost and abundant resource is an important social and economic strategy. Waste biomass is a promising candidate to produce AC with mass production and low cost. Currently, some pioneering work has been systematically investigated in waste biomass, such as tea leaf, chicken eggshell, rice husk, straw and coconut shell, showing promising prospect for AC production [9–13].

Potato is one of the most important crops around the world except the rice and wheat because of its high yield, strong adaptability and low production cost [14], and numerous tons of rotten potatoes produced in the

manufacturing and selling process. A roughly estimated 22 % of potatoes (65 million tons) are lost the value of food due to the deterioration by viral, bacterial or fungal diseases and pests [15]. Rotten potatoes are normally buried in the soil, burned or thrown away in somewhere else, which not only causes serious environmental pollution but also a wasting of resource. Thus, to fabricate AC derived from waste rotten potatoes is a significantly environmental and economic friendly way due to the low cost and high additional value. Potato starch was used as raw material for high-performance electric double-layer capacitor since 2012 [16], however, it is not suitable for practice application.

In this work, we have fabricated porous AC derived from waste rotten potatoes by hydrothermal reaction, carbonization and activation process. The as-obtained AC owns high specific area (960 m^2 g^{-1}), and a pore size distribution in both micropore and mesopore arranges. The formed AC with large specific area shows good specific capacitance as high as 269 F g^{-1} at the current density of 1 A g^{-1}, excellent rate performance (55.3 % the capacitance was retained when current density is increased from 1 to 100 A g^{-1}) and long cycle life (only 5 % capacitance loss after 7000 cycles). Furthermore, the symmetric button cell devices fabricated based on the rotten potatoe-derived AC present a high specific capacitance, considerable energy density as well as perfect cycling stability. All above-mentioned results imply that the rotten potatoes could be of a valuable and potential precursor for high-performance AC used as EDLCs electrode materials.

Materials and Methods

Sample Preparation

Rotten potatoes gathered from local family were first washed thoroughly and cut into pieces, followed by hydrothermal process at 200 °C for 8 h. The hydrothermal products were washed with deionized water for several times and dried in vacuum furnace at 80 °C. After drying, the samples were mixed with KOH at the mass ratio of 1:1 and heated to 750 °C at heating rate of 5 °C min^{-1} and kept for 1 h. The product was washed with 1 M HCl and distilled water thoroughly for several times until the pH of washing liquid was neutral, and then it was dried at 100 °C. For comparison, the non-activated carbon (NAC) was prepared in the similar procedures but without adding KOH during the annealing process.

Sample Characterization

The morphology and structure of the samples were characterized by field emission scanning electron microscopy (FE-SEM, FEI Nova 430 Nano) using an accelerating voltage of 20 kV and Raman spectra (HR RamLab) with the 514.5 nm Ar^+ laser as the excitation source. The surface area and pore size distribution were evaluated using N_2 adsorption (Micromeritics, ASAP 2020 analyzer). The specific surface area was calculated from the N_2 adsorption isotherm based on the Brunauer–Emmett–Teller (BET) equation. The pore size distribution was calculated based on the adsorption branches of the isotherms by Barrett–Joyner–Halenda (BJH) analysis method.

Electrochemical Evaluation

AC or NAC derived from rotten potatoes, polytetrafluoroethylene (PTFE) binder and acetylene black were first mixed with the mass ratio of 8:1:1 using ethanol as dispersant. The obtained mixed slurry was sprayed on Ni foam plates (1 cm × 1 cm) by doctor-blade technique, followed by fully drying in oven at 60 °C for 12 h. The mass loading of the active material of electrode was about 2.00 mg cm^{-2}. The electrochemical performances of the working electrode containing AC and NAC were measured on electrochemical work station (CHI 660c) in three electrode systems, a saturated calomel electrode (SCE) and a carbon plate as the reference electrode and countering electrode, respectively. The measurement was taken in a 6 M KOH solution. Cyclic voltammetry (CV) was performed from −1 to −0.2 V (vs. SCE) at different scan rates from 50 to 400 mV s^{-1}. Galvanostatic charge/discharge (GCD) curves were measured at different current densities from 1 to 100 A g^{-1} under the potential range from −1 to −0.2 V (vs. SCE). Furthermore, the symmetric button capacitor was assembled with two pieces of working electrodes separated by a layer of polypropylene membrane. CV and GCD performance of the AC-based symmetric device was collected at different scan rates from 10 to 200 mV s^{-1} and different current densities from 1 to 100 A g^{-1} within the potential range of 0–0.8 V.

Results and Discussion

Scheme 1 shows digital pictures about the fabrication process of the AC. Firstly, brown product is obtained after hydrothermal treatment of rotten potato at 200 °C for 8 h (Scheme 1b). Then, the uniform black AC with a mass yield of 8.7 % (Scheme 1c) is obtained after KOH activation treatment of the hydrothermal product. Without

Scheme 1 The preparation process of porous AC. **a** Raw rotten potato. **b** The product of rotten potato after hydrothermal treatment at 200 °C for 8 h. **c** AC

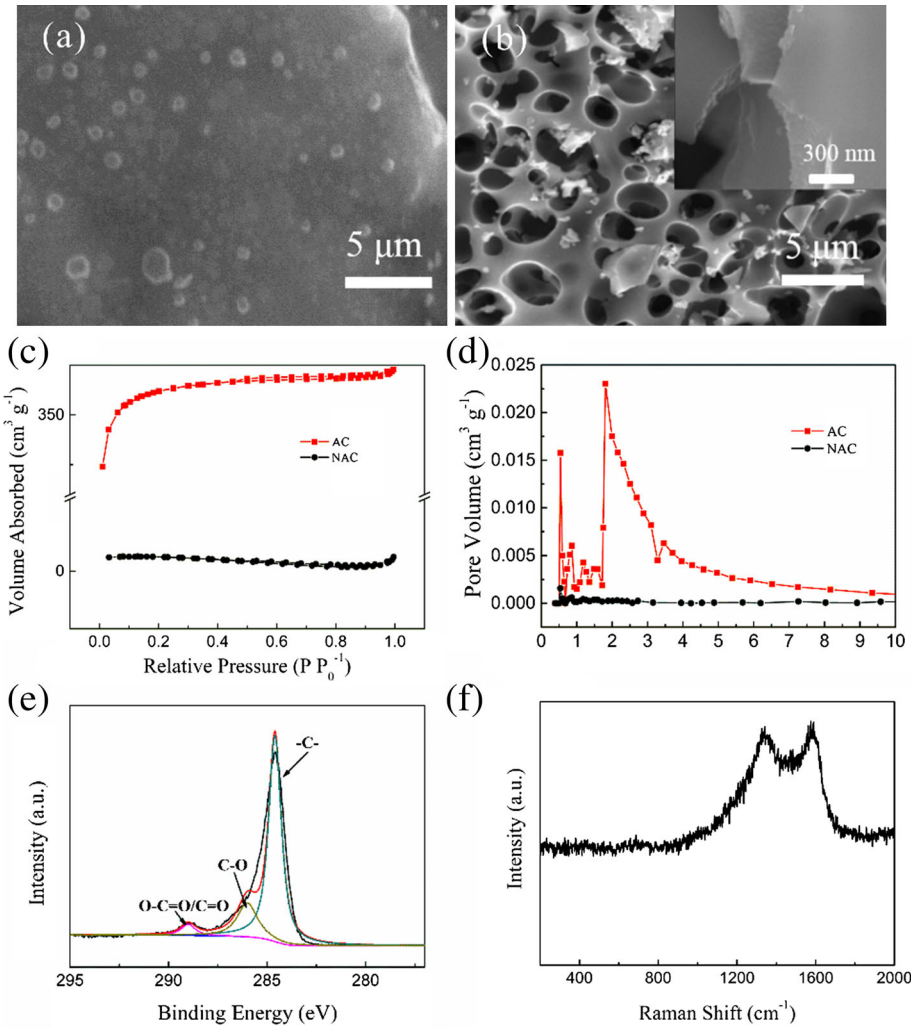

Fig. 1 SEM images of NAC (**a**) and AC (**b**). The N_2 adsorption isotherm (**c**) and pore size distribution profiles (**d**) of NAC and AC. High-resolution XPS spectra of C1s (**e**) and Raman shift spectra (**f**) collected for AC

activation treatment, the product shows smooth surface, as shown in Fig. 1a. Figure 1b shows the low- and high-magnification (insert picture) SEM images of the AC synthesized by hydrothermal reaction and the following activation of KOH. It is obvious that large amounts of macropore with about 1–3 μm in diameter were formed continuously. The rough surface of AC is observed in the high-resolution SEM image (insert in Fig. 1b) suggesting the existence of mesopore. Specific surface area of AC is as high as 960 $m^2\ g^{-1}$ and much larger than that of NAC (14 $m^2\ g^{-1}$) (Fig. 1c). The corresponding pore size distribution is also performed to characterize the porosity of AC and NAC, as shown in Fig. 1d. In comparison with NAC, AC presents the mixed type I and IV isotherm defined by the International Union of Pure and Applied Chemistry (IUPAC), and the classification reveals the coexistence of both microporous and mesoporous structures in AC [17, 18]. The insert in Fig. 1d depicts that AC owns two narrow peaks centered at 2–5 and 1 nm confirming that the AC has amount of micropores and mesopores, which is promising structure for the high-performance EDLC electrode materials. The fine X-ray

photoelectron spectroscopy (XPS) spectrum of the carbon element (C1s) collected for AC is investigated to determine the chemical component and its electric state (Fig. 1e). It is obvious that the original curve can be fitted by three different peaks located at 284.6, 285.2 and 289.0 eV which can be attributed to graphitic carbon, aliphatic carbon and carboxyl and/or ester groups [19]. Figure 1f presents the Raman spectra of AC, and two representative peaks located at 1598 and 1345 cm^{-1} can be assigned to the hexagonal carbon plane (G band) and crystal defects or imperfections indicating formation of carbon elementary substance with high disordered structures [20].

Figure 2a presents the CV curves of AC and NAC measured at the scanning rate of 50 mV s^{-1} within the potential range from −0.2 to −1 V in three electrode systems. The shape of CV curve collected for AC is approximatively rectangular, and the enclosed area is much larger than that of NAC, indicating the excellent electrochemical performance of AC. GCD curves based on AC and NAC are shown in Fig. 2b, indicating that the specific capacitance of AC is as high as 269 F g^{-1} at the current density of 1 A g^{-1} which is much larger than that of NAC according to the following equation [21–23].

$$C = \frac{I \times \Delta t}{m \times \Delta V} \quad (1)$$

where C (F g^{-1}) stands for specific capacitance, I is the current of charge and discharge process, m is the mass of the active material, Δt (s) is the discharge time, and ΔV (V) is the potential range.

Figure 2c depicts the CV curves of the AC at different scan rates from 5 to 400 mV s^{-1} within the voltage range from −1 to −0.2 V (vs. SCE). All CV curves exhibit nearly rectangular shape even at a high scanning rate of 400 mV s^{-1}, indicating good capacitive performance. GCD plots (Fig. 2d) show symmetric triangle shapes without any obvious voltage drop at current density from 1 to 20 A g^{-1}, revealing excellent EDLC capacitive behavior. The specific capacitance was calculated to be 269, 255, 239, 231 and 215 F g^{-1} at current density of 1, 2, 5, 10 and

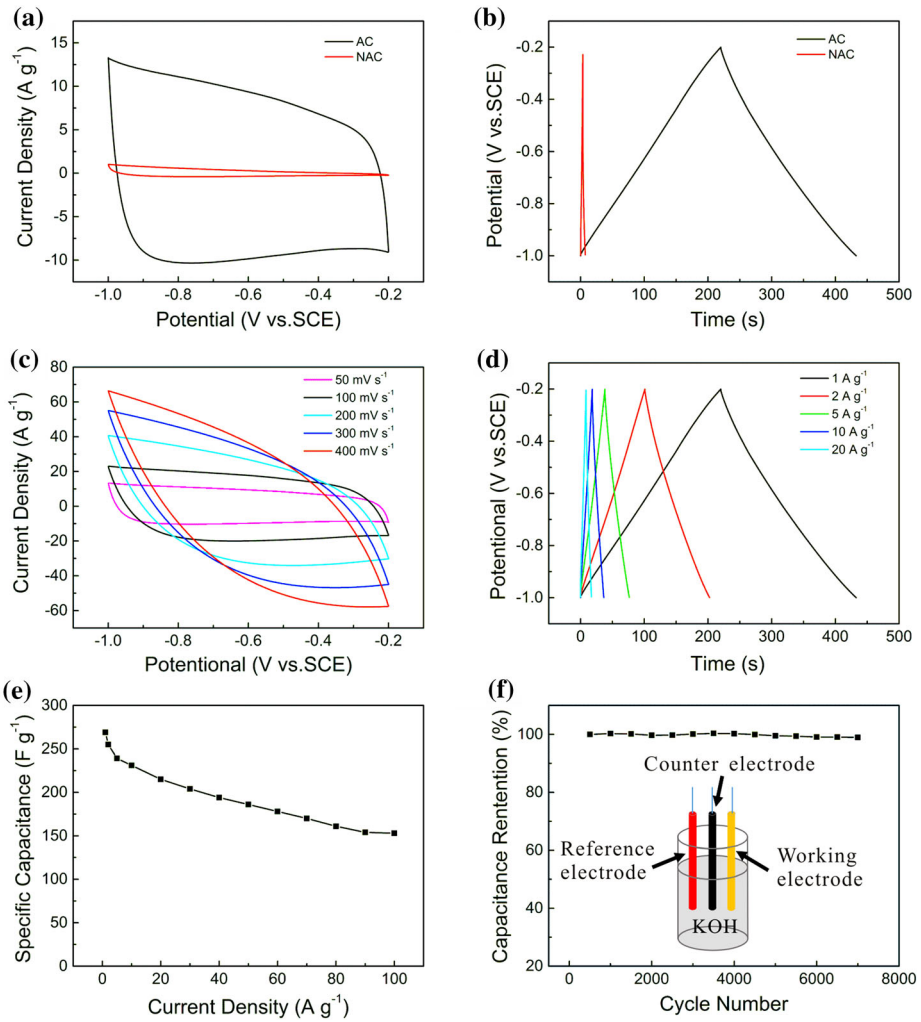

Fig. 2 **a** The CV curves of NAC and AC at the scanning rate of 50 mV s^{-1}. **b** The GCD curves of NAC and AC at current density of 1 A g^{-1}. **c** The CV curves at different scan rates from 50 to 400 mV s^{-1} for AC. **d** The GCD curves of the AC at different current densities from 1 to 20 A g^{-1}. **e** The rate capability of AC. **f** Cycle life performance detected by CV at the scan rate of 100 mV s^{-1}.

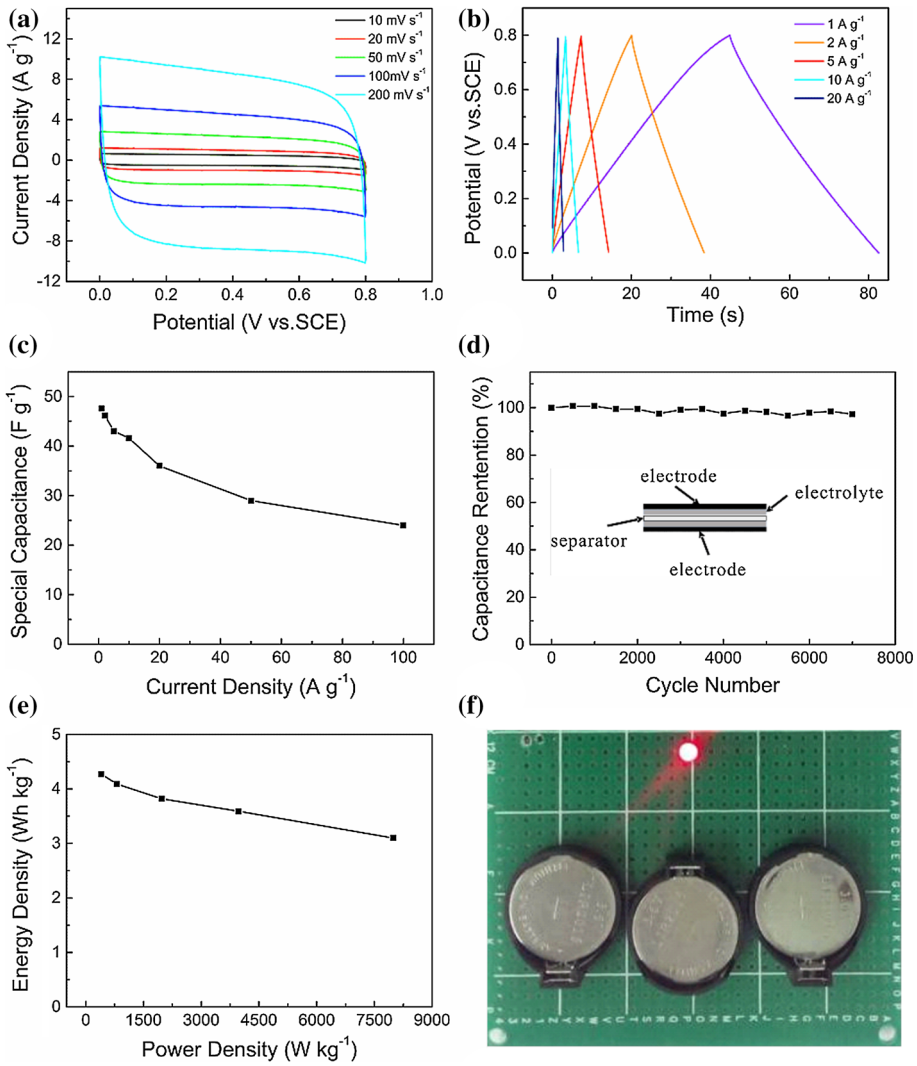

Fig. 3 **a** The CV curves at different scan rates from 10 to 200 mV s^{-1}. **b** The GCD curves at different current densities from 1 to 20 A g^{-1} collected for AC-based symmetric device. **c** The rate capability of AC-based symmetric supercapacitive device. **d** The Cycle performance of AC-based symmetric device detected by CV at the scan rate of 100 mV s^{-1}. **e** The relationship of energy density and power density collected for AC-based symmetric device. **f** The Digital picture of the red LED bulb powered by three AC-based symmetric devices in series

20 A g^{-1}, respectively. It is obvious that the capacitance retention is 85 % (215 F g^{-1}) when the current density is increased 20 times. When increased to 100 A g^{-1} (Fig. 2e), the capacitance still remains 55.7 % (152 F g^{-1}). The rate performance of rotten potato is better than recent results, such as AC derived from loofah sponge (60.2 % capacitance retention at a current density of 50 A g^{-1}) and waste tobacco recycled carbon (the capacitance keeps approximately 54 % when the current density is increased 20 times) [24, 25], indicating the high rate performance of the rotten potato-based AC. Cycling stability of AC electrode is also tested at a scanning rate of 100 mV s^{-1} in 6 M KOH solution within the potential range from −1 to −0.2 V (vs. SCE) (Fig. 2f). The capacitance retains more than 95 % initial capacitance after 7000 cycles indicating excellent long-term life performance. The outstanding supercapacitive performance of the AC can be attributed to the continuously interconnected 3D micro-/meso-/macroporous structure as well as considerable conductivity.

The symmetric capacitor is assembled with two same pieces of active electrode and a layer of polypropylene membrane as separator and sealed in button coin cell. The electrochemical performance of the symmetric device is measured within the potential range from 0 to 0.8 V. Figure 3a presents the CV curves of the button cell at different scan rates from 10 to 200 mV s^{-1}. The highly regular rectangle shapes at different scan rates of 10 to 200 mV s^{-1} are observed which indicates the excellent capacitance of the device. GCD curves measured at different current densities from 1 to 20 A g^{-1} under the potential range of 0–0.8 V are shown in Fig. 3b. The specific capacitance of the device is calculated by Eq. (1), which reaches up to 48, 46, 43, 41 and 36 F g^{-1} at a current density of 1, 2, 5, 10 and 20 A g^{-1}, respectively.

And the specific capacitance of the symmetric device retains about 53 % when the current density is increased from 1 to 100 A g^{-1} (Fig. 3c), which is larger than that fabricated symmetric device based on carbon materials derived from human hair [26], enteromorpha prolifera [27], orange peel [28] and seaweed [29]. Figure 3d shows the cycling performance of fabricated symmetric device measured at the scanning rate of 100 mV s^{-1} under the potential range from 0 to 0.8 V. Without visible decay can be observed after 7000 cycles demonstrating the extraordinary long-term cycling life of the symmetric device based on the rotten potatoe-derived carbon. Ragone plot related to energy density and the power density is an efficient way to evaluate the capacitive performance of supercapacitors. The energy density (E) and the power density (P) can be calculated by the following equations:

$$E = 0.5CV^2 \quad (2)$$

$$P = \frac{E}{t} \quad (3)$$

The assembled symmetric supercapacitor delivers a maximum energy density of 4.27 Wh kg^{-1} and power density of 405.60 W kg^{-1} at the current density of 1 A g^{-1} (Fig. 3e). The red light emitting diode (LED) with threshold voltage of 1.8 V can be driven for at least 10 s (Fig. 3f) by three button coin cells in series, indicating the good feasibility of the rotten potatoe-derived carbon materials in EDLC supercapacitive device.

Conclusions

In summary, high electrochemical performance of AC with specific area of 960 m^2 g^{-1} and micro-/meso-/macropore structure has been successfully synthesized by environmentally hydrothermal treatment of rotten potatoes at 200 °C and KOH activation in 750 °C in succession. The obtained AC exhibits high specific capacitance of 269 F g^{-1} at a current density of 1 A g^{-1}, excellent rate performance with a capacitance retention of 55.7 % when the current density is increased 100 times and good stability with only capacitance decay of 5 % after 7000 cycles. In addition, the assembled symmetric capacitor based on the rotten potatoes-derived AC shows high specific capacitance of 48 F g^{-1} and considerable energy density of 4.27 Wh Kg^{-1} at a current density of 1 A g^{-1}. The result offers a facile, low-cost and environmentally friendly approach to fabricate high-capacitive carbon materials for commercial EDLC-related applications.

Acknowledgments This work was financially supported by Natural Science Foundation of China (51504171 and 5157210), the project of Hubei Provincial Education Office (B2015346), the outstanding young and middle-aged scientific innovation team of colleges and universities of Hubei Province (T201402), and the applied basic research program of Wuhan City (2013011801010598).

References

1. Liu, R.L., Wan, L., Liu, S.Q., Pan, L.X., Wu, D.Q., Zhao, D.Y.: Supercapacitors: an interface-induced co-Assembly approach towards ordered mesoporous carbon/graphene aerogel for high-performance supercapacitors. Adv. Funct. Mater. **25**(4), 651 (2015)
2. Du, P., Hu, X., Yi, C., Liu, H.C., Liu, P., Zhang, H.L., Gong, X.: Self-powered electronics by integration of flexible solid-state graphene-based supercapacitors with high performance perovskite hybrid solar cells. Adv. Funct. Mater. **25**(16), 2420–2427 (2015)
3. Zhou, J., Zhu, T.T., Xing, W., Li, Z.H., Shen, H.L., Zhuo, S.P.: Activated polyaniline-based carbon nanoparticles for high performance supercapacitors. Electrochim. Acta **160**, 152–159 (2015)
4. Chen, G.F., Su, Y.Z., Kuang, P.Y., Liu, Z.Q., Chen, D.Y., Wu, X., Qiao, S.Z.: PolypyrroleShell@ 3D-Ni metal core structured electrodes for high-performance supercapacitors. Chem. Eur. J. **12**(21), 4614–4621 (2015)
5. Haas, O., Cairns, E.J.: Electrochemical energy storage. Annu. Rep. Prog. Chem. Sect C: Phys. Chem. **95**, 163–198 (1999)
6. Zheng, C., Zhou, X.F., Cao, H.L., Wang, G.H., Liu, Z.P.: Synthesis of porous graphene/activated carbon composite with high packing density and large specific surface area for supercapacitor electrode material. J. Power Sources **258**, 290–296 (2014)
7. Lin, Z.Y., Yan, X.B., Lang, J.W., Wang, R.T., Kong, L.B.: Adjusting electrode initial potential to obtain high-performance asymmetric supercapacitor based on porous vanadium pentoxide nanotubes and activated carbon nanorods. J. Power Sources **279**, 358–364 (2015)
8. Qian, W.J., Zhu, J.Y., Zhang, Y., Wu, X., Yan, F.: Condiment-derived 3D architecture porous carbon for electrochemical supercapacitors. Small (2015). doi:10.1002/smll.201500859
9. Peng, C., Yan, X.B., Wang, R.T., Lang, J.W., Ou, Y.J., Xue, Q.J.: Promising activated carbons derived from waste tea-leaves and their application in high performance supercapacitors electrodes. Electrochim. Acta **87**, 401–408 (2013)
10. Li, Z., Zhang, L., Amirkhiz, B.S., Tan, X., Xu, Z., Wang, H., Olsen, B.C., Holt, C.M.B., Mitlin, D.: Carbonized chicken eggshell membranes with 3D architectures as high-performance electrode materials for supercapacitors. Adv. Energy Mater. **2**(4), 431–437 (2012)
11. He, X.J., Ling, P.H., Yu, M.X., Wang, X.T., Zhang, X.Y., Zheng, M.D.: Rice husk-derived porous carbons with high capacitance by $ZnCl_2$ activation for supercapacitors. Electrochim. Acta **105**, 635–641 (2013)
12. Li, X.L., Han, C.L., Chen, X.Y., Shi, C.W.: Preparation and performance of straw based activated carbon for supercapacitor in non-aqueous electrolytes. Microporous Mesoporous Mater. **131**(1), 303–309 (2010)
13. Dandekar, M.S., Arabale, G., Vijayamohanan, K.: Preparation and characterization of composite electrodes of coconut-shell-based activated carbon and hydrous ruthenium oxide for supercapacitors. J. Power Sources **141**(1), 198–203 (2005)
14. Bovell-Benjamin, A.C.: Sweet potato: a review of its past, present, and future role in human nutrition. Adv. Food Nutr. Res. **52**, 1–59 (2007)
15. Czajkowski, R., Pérombelon, M.C.M., van Veen, J.A., van der Wolf, J.M.: Control of blackleg and tuber soft rot of potato

caused by pectobacterium and dickeya species: a review. Plant Pathol. **60**(6), 999–1013 (2011)
16. Li, Q.Q., Liu, F., Zhang, L., Nelson, B.J., Zhang, S.H., Ma, C., Tao, X.Y., Cheng, J.P., Zhang, X.B.: In situ construction of potato starch based carbon nanofiber/activated carbon hybrid structure for high-performance electrical double layer capacitor. J. Power Sources **207**, 199–204 (2012)
17. Ma, X., Ouyang, F.: Adsorption properties of biomass-based activated carbon prepared with spent coffee grounds and pomelo skin by phosphoric acid activation. Appl. Surf. Sci. **268**, 566–570 (2013)
18. Torchała, K., Kierzek, K., Gryglewicz, G., Machnikowsk, J.: Narrow-porous pitch-based carbon fibers of superior capacitance properties in aqueous electrolytes. Electrochim. Acta **167**, 348–356 (2015)
19. Cai, T.H., Xing, W., Liu, Z., Zeng, J.B., Xue, Q.Z., Qiao, S.B., Yan, Z.F.: Superhigh-rate capacitive performance of heteroatoms-doped double shell hollow carbon spheres. Carbon **86**, 235–244 (2015)
20. Kaufman, J.H., Metin, S., Saperstein, D.D.: Symmetry breaking in nitrogen-doped amorphous carbon: infrared observation of the Raman-active G and D bands. Phys. Rev. B **39**(18), 13053 (1989)
21. Lee, H.M., Jeong, G.H., Kang, D.W., Kim, S.W., Kim, C.K.: Direct and environmentally benign synthesis of manganese oxide/graphene composites from graphite for electrochemical capacitors. J. Power Sources **281**, 44–48 (2015)
22. Fu, W.D., Long, L., Wang, M., Yao, Y.D., Wei, N.D., Yan, M.L., Yin, G.F., Liao, X.M., Huang, Z.B., Chen, X.C.: Pine needle β-Co $(OH)_2$ grown on Ni foam substrate for high specific capacitance and good cycling stability as advanced electrochemical pseudocapacitor materials. J. Alloys Compd. **631**, 82–85 (2015)
23. Yan, J., Wang, Q., Wei, T., Fan, Z.J.: Recent advances in design and fabrication of electrochemical supercapacitors with high energy densities. Adv. Energy Mater. **4**, 1300816 (2014)
24. LuanY, T., Wang, L., Guo, S.E., Jiang, B.J., Zhao, D.D., Yan, H.J., Tian, C.G., Fu, H.G.: Hierarchical porous carbon material from network loofah sponge for high performance supercapacitors. RSC Adv. **5**, 42430–42437 (2015)
25. Sha, Y.F., Lou, J.Y., Bai, S.Z., Wu, D., Liu, B.Z., Ling, Y.: Facile preparation of nitrogen-doped porous carbon from waste tobacco by a simple pre-treatment process and their application in electrochemical capacitor and CO_2 capture. Mater. Res. Bull. **64**, 327–332 (2015)
26. Qian, W.J., Sun, F.X., Xu, Y.H., Qiu, L.H., Liu, C.H., Wang, S.D., Yan, F.: Human hair-derived carbon flakes for electrochemical supercapacitors. Energy Environ. Sci. **7**(1), 379–386 (2014)
27. Gao, L., Xing, W., Zhou, J., Wang, G.Q., Zhuo, S.P., Liu, Z., Xue, Q.Z., Yan, Z.F.: Superior capacitive performance of active carbons derived from enteromorpha prolifera. Electrochim. Acta **133**, 459–466 (2014)
28. Sun, K.J., Wang, H.P., Peng, H., Wu, Y.J., Ma, G.F., Lei, Z.Q.: Manganese oxide nanorods supported on orange peel-based carbon nanosheets for high performance supercapacitors. Int. J. Electrochem. Sci. **10**, 2000–2013 (2015)
29. Wu, X.Z., Xing, W., Florek, J., Zhou, J., Wang, G.Q., Zhuo, S.P., Xue, Q.Z., Yan, Z.F., Kleitz, F.: On the origin of the high capacitance of carbon derived from seaweed with an apparently low surface area. J. Mater. Chem. A **2**, 18998–19004 (2014)